


Measurement of $^{39}\text{K}(p, \gamma)^{40}\text{Ca}$ resonance strengths below 900 keV for nucleosynthesis in classical novae

Philipp Scholz,^{*} Richard J. deBoer[✉], Joachim Görres, August Gula,[†] Rebecca Kelmar, Khachatur Manukyan[✉], Edward Stech, Wanpeng Tan, and Michael Wiescher[✉]

Department of Physics and Astronomy and the Joint Institute for Nuclear Astrophysics, University of Notre Dame, Notre Dame, Indiana 46556, USA

 (Received 28 February 2023; revised 2 May 2023; accepted 12 June 2023; published 20 June 2023)

Classical novae are one of the most frequent explosive nucleosynthesis events in our universe but are still not sufficiently understood. To this day, nuclear astrophysics cannot explain the endpoint of the nucleosynthesis networks that drive them. This is mainly due to a scarce experimental database of nuclear reaction rates for proton induced reactions in the mass region above silicon at temperatures between 0.1 and 0.4 GK. Because some nova ejecta hint at the production of elements in the calcium range (Centauri V1065), and some possibly even up to the iron region (Cygni V1974), it is of utmost interest to investigate possible paths towards heavier elements. Here we report on new measurements of resonance strengths for the $^{39}\text{K}(p, \gamma)^{40}\text{Ca}$ reaction below 900 keV. Measurements were performed at the 5U accelerator at the University of Notre Dame. The implications of these new strengths for the $^{39}\text{K}(p, \gamma)^{40}\text{Ca}$ reaction rate are discussed.

DOI: [10.1103/PhysRevC.107.065806](https://doi.org/10.1103/PhysRevC.107.065806)

I. INTRODUCTION

Novae are explained as thermonuclear explosions under highly degenerate conditions on the surface of an accreting white dwarf in a binary star system [1]. The explosive hydrogen burning is driven by the mixing of the accreted hydrogen and helium rich material from the outer envelope of the companion star with the white dwarf surface matter, subsequently causing ignition through nuclear fusion reactions. The associated energy release under highly degenerate conditions causes a rapid temperature increase, an exponential increase in reaction rates and, subsequently, a rapid conversion of the white dwarf surface material to heavier mass elements. The actual nuclear reaction sequence driving the thermonuclear runaway depends on the nature of the white dwarf star and its surface composition.

A carbon-oxygen white dwarf star, formed after stellar helium burning, is characterized by a predominantly carbon and oxygen composition and the thermonuclear runaway is driven by the hot CNO cycles, with most of the initial ^{12}C and ^{16}O material redistributed to ^{14}N , ^{15}N , as well as ^{18}O , which is mostly ejected in the nova explosion [2]. As shown recently, there may be leakage from the CNO cycles towards the Ne-Na cycle through the $^{19}\text{F}(p, \gamma)^{20}\text{Ne}$ reaction [3], but the full impact of this leakage for classical novae has not yet been fully explored.

An oxygen-neon white dwarf, formed after stellar carbon burning, is characterized by an oxygen, neon, and magnesium composition. The thermonuclear explosion is driven by the

Ne-Na cycle and the subsequent Mg-Al cycle, which are linked by the $^{23}\text{Na}(p, \gamma)^{24}\text{Mg}$ reaction [4]. This cyclic pattern branches into a continuous reaction flow, converting the initial fuel distribution through a sequence of proton capture reactions into the S/Ca mass range as observed in nova ejecta. In the lower mass range, between Ne and Si, the production of long-lived radioisotopes such as ^{22}Na and ^{26}Al is anticipated as a result of the hot Ne-Na and Mg-Al cycles. The reaction path in the higher mass range runs close to the line of stability, since the temperatures of the thermonuclear runaway are not high enough for the proton capture reaction rates to compete with the β^+ decay of the short lived neutron deficient nuclei. The reaction path is also increasingly dominated by radiative capture (p, γ) reactions while competing (p, α) processes, such as $^{31}\text{P}(p, \alpha)^{28}\text{Si}$ and $^{35}\text{Cl}(p, \alpha)^{32}\text{S}$, are, with increasing Z , suppressed by the Coulomb barrier of the emitting α particles [5].

The endpoint of the nucleosynthesis path is not well defined and depends on the temperature and density development during the runaway, namely the transition from a degenerate to an ideal gas condition in the environment. This would cause rapid expansion and cooling, halting the nuclear reaction processes. On the other hand, the endpoint also depends on the rates of the radiative capture reactions and β^+ decays along the reaction path. Previous reaction studies above ^{28}Si have primarily focused on radiative capture on ^{31}P [6], ^{32}S [7], ^{35}Cl [8], and ^{36}Ar [9]. Subsequent simulations of nova nucleosynthesis indeed confirmed that the reaction pattern may well expand into this mass range [10].

Spectroscopic observations, however, also show indications for the existence of heavier nuclei such as Ca, Mn, and Fe in the ejecta [11,12]. These elements appear in spurious amounts but the observation indicates that there may be a nucleosynthesis path towards heavier nuclei beyond the *sd*

^{*}Present address: Capgemini Engineering, München, Germany.

[†]Present address: Los Alamos National Laboratory MS-D436, P.O. Box 1663, Los Alamos, NM 87545-0001.

shell in nova environments. There is only limited information about the reaction rates for proton capture processes in this mass range. A frequent assumption is that high level density in the compound nucleus justifies the application of statistical models, but the level density in closed shell nuclei, such as ^{40}Ca , is substantially lower. We therefore undertook a direct study of the $^{39}\text{K}(p, \gamma)^{40}\text{Ca}$ reaction at low energies with the aim of better understanding the reaction flow at the closure of the *sd* shell for explosive hydrogen burning.

II. PREVIOUS MEASUREMENTS

The $^{39}\text{K}(p, \gamma)^{40}\text{Ca}$ reaction has been studied primarily to investigate the level structure of the doubly closed shell nucleus ^{40}Ca . Direct radiative capture measurements, in particular, provided information about states above the proton threshold, which appear as resonances in the radiative proton capture cross section. Initial studies, such as those by Leenhouts and Endt [13], Leenhouts [14], and Cheng *et al.* [15], primarily provided level information at proton energies above 1 MeV, well above the energy range of interest for explosive hydrogen burning. A more recent study by Kikstra *et al.* [16] expanded these measurements, probing substantially lower proton energies and revealed the existence of several resonances above 600 keV that could provide important contributions to the reaction rate. This was further underlined by an unpublished study of low energy resonances at the University of Notre Dame [17].

In the following, we first discuss the experimental arrangements and conditions for a new measurement of the $^{39}\text{K}(p, \gamma)^{40}\text{Ca}$ reaction performed at the University of Notre Dame. This is followed by a discussion of the observed levels in the context of the level structure of ^{40}Ca as observed through single-particle transfer reactions such as $^{39}\text{K}(d, n)^{40}\text{Ca}$ [18], and $^{39}\text{K}(^3\text{He}, d)^{40}\text{Ca}$ [19–21]. These data provide complementary information about the single-particle strength distribution near the proton threshold of the closed shell nucleus ^{40}Ca within the Gamow range of explosive hydrogen burning, as indicated in Fig. 1.

Based on information available before the present work, a new evaluation of the reaction was performed by Longland *et al.* [22]. The authors took into account a number of discrepancies in the previous results by means of a Monte Carlo analysis after renormalizing the various resonance strengths to that at $E_r^{\text{c.m.}} = 1.990$ MeV given by Cheng *et al.* [15]. Longland *et al.* [22] also suggested a considerably larger number of resonances below the energy range of direct measurements based on observations from transfer studies. With our work, we seek to reduce the uncertainties in the previously measured resonance parameters and to investigate the presence of resonances that, as yet, have not been observed directly. Finally, we will discuss our experimental results and analyze the contributions to the reaction rate for nova burning.

III. EXPERIMENTAL GOALS AND ARRANGEMENTS

The goal of this experimental study is to map the excitation curve of the $^{39}\text{K}(p, \gamma)^{40}\text{Ca}$ reaction over the proton energy range below 1 MeV in order to determine the strengths of

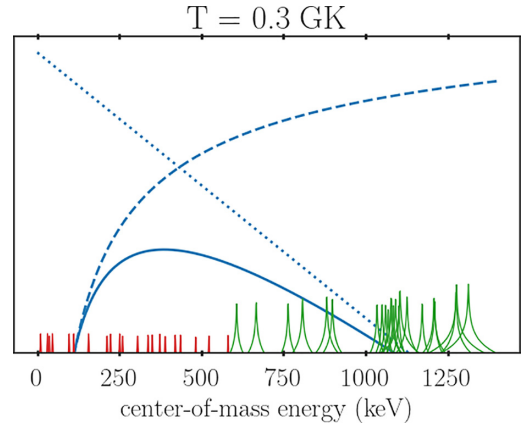


FIG. 1. The figure illustrates the energy dependence of the Gamow peak for $T = 0.3$ GK for the reaction $^{39}\text{K}(p, \gamma)^{40}\text{Ca}$ (solid line) as defined by the Maxwell-Boltzmann distribution of the interacting particles (dotted line) and the proton penetrability through the Coulomb barrier (dashed line) with the single-particle strength distributions of the observed proton unbound states in ^{40}Ca . Directly observed and candidate states [22] are indicated by green Breit-Wigner shapes and red vertical lines, respectively.

the previously observed low energy resonances [16,17] with improved precision and to observe additional resonances predicted by transfer measurements. The level density in ^{40}Ca above the proton threshold ($S_p = 8.328$ MeV) is rather high, as argued by Longland *et al.* [22], with an average level spacing of ≈ 20 keV, but many of the suggested levels have either high spins, which would substantially reduce their resonance strength due to the high orbital momentum barrier, or are simply too far outside the Gamow energy range of explosive hydrogen burning to be of any relevance. Due to the high Coulomb and orbital angular momentum barrier and the absence of other particle decay channels, all of the resonances are very narrow, having total widths well below 1 meV [23]. Interference effects are therefore negligible and the reaction rate can be calculated with sufficient accuracy using the narrow resonance approximation [24]

$$\langle \sigma v \rangle = \left(\frac{2\pi}{\mu kT} \right)^{3/2} \sum_i (\omega \gamma_i) \hbar^2 \exp\left(-\frac{E_i}{kT}\right), \quad (1)$$

which depends only on the energies E_i and the strengths $\omega \gamma_i$ of the observed resonances. The former are well known from previous studies (see Longland *et al.* [22] and references therein), while the latter can be directly determined from the thick target yield of the resonances [25]. Since the observed yield depends directly on the target stability, the largest handicap in previous measurements has been target deterioration under the intense proton beam bombardment necessary to obtain appreciable yields [17].

The experiment was divided into three phases. First, the resonances above 600 keV were mapped out with a thin target. Second, long measurements on top of the respective thick-target yield plateaus were performed in order to obtain precise measurements of the resonance strengths. Finally, thicker

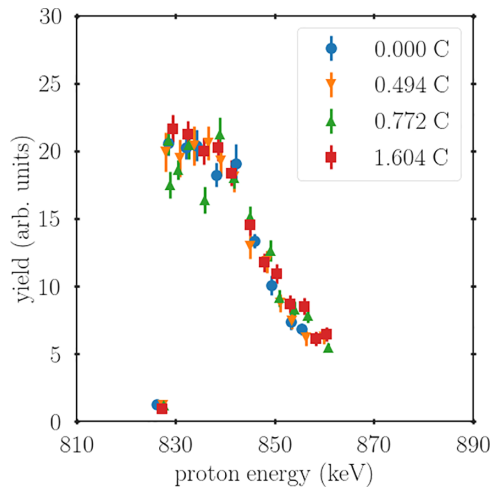


FIG. 2. During long measurements, on top of the known resonances, the stability of the thin targets was monitored by scanning the $E_p = 828$ keV resonance of the $^{39}\text{K}(p, \gamma)^{40}\text{K}$ reaction. The scans revealed no measurable degradation.

targets were used to search for new resonances in the region below 600 keV using long irradiation times.

A. Target production and characterization

The KI targets previously used in other studies [16,17] showed rapid deterioration and therefore limited the accuracy of the resonance strength measurements using the thick target technique. For the present experiment, a new potassium target composition of K_2WO_4 was used with 99.5% purity and natural K abundance (93.258% ^{39}K , 0.012% ^{40}K , and 6.730% ^{41}K). The target material was evaporated onto tantalum backings of 0.3 mm thickness. The tantalum backings were cleaned by successive sonication in acetone, ethanol, and isopropanol for 10 min at each step, followed by drying under an argon flow. The backings were vacuum annealed (at 5×10^{-6} torr) by electric current heating to $\approx 700^\circ\text{C}$ before the K_2WO_4 material was evaporated with a deposition rate of 0.5 nm/s until the desired target thickness was reached. The targets exhibited high stability during the experiment without significant degradation.

Targets with two different thicknesses were used in the present experiment: (i) $100 \mu\text{g}/\text{cm}^2$ with an approximate energy loss of 25 keV at $E_p = 600$ keV to map out the resonances after they had been identified, either from previous direct measurements or from the present thick-target measurements, and (ii) $500 \mu\text{g}/\text{cm}^2$ thick targets to investigate and explore resonances below $E_p = 600$ keV. Throughout the measurements, the stability of the thinner targets were monitored using the $E_r = 828$ keV resonance in the $^{39}\text{K}(p, \gamma)^{40}\text{Ca}$ reaction; see Fig. 2. Compared to the earlier measurements of Kikstra *et al.* [16], Cheng *et al.* [15], and Meißner [17], where KI targets were used, the K_2WO_4 target material was observed to have much improved stability, even after accumulating several Coulombs of charge. The stability of the thicker targets were monitored by the yield on the plateau of the $E_p = 622$ keV resonance. However, the analysis was hampered by a

number of background lines in the γ spectra from the reactions $^{12}\text{C}(p, \gamma)^{13}\text{N}$, $^{19}\text{F}(p, \alpha\gamma)^{16}\text{O}$, and $^{23}\text{Na}(p, \alpha\gamma)^{20}\text{Ne}$, which came from target impurities such as ^{19}F in the tantalum backing and ^{12}C and ^{23}Na in the target material, respectively. Also observed were lines from $^{16}\text{O}(p, \gamma)^{17}\text{F}$ from the oxygen component in the target material. Finally we observed γ transitions from the $^{41}\text{K}(p, \gamma)^{42}\text{Ca}$ reaction on the small ^{41}K isotopic component in the target since it was not possible to get ^{39}K enriched target material. However, the background issue was of secondary importance since the γ transitions coming from the $^{39}\text{K}(p, \gamma)^{40}\text{Ca}$ reaction are well known and could easily be identified on the basis of their energies and energy shifts with respect to the beam energy.

B. Experimental details

The measurements were performed using the 5U Pelletron accelerator of the Nuclear Science Laboratory at the University of Notre Dame over the proton laboratory energy range between $E_p = 0.4$ and 1.4 MeV. The energy calibration of the beam was determined using the energies of well known resonances in the $^{27}\text{Al}(p, \gamma)^{28}\text{Si}$ reaction [26], and was determined to better than 1 keV over the energy range of the present measurements. The main goal of the present study was to measure the on-resonance yield of strong resonances with high accuracy to verify the resonance strength predictions by Longland *et al.* [22]. For this purpose the targets were mounted at 45° relative to the beam direction to suppress effects due to angular distribution. To reduce degradation from beam heating, the target backings were directly water-cooled. A circular copper tube was mounted inside the beam line, which extended from a liquid nitrogen cooled cold head to within a few millimeters of the target face. The copper tube was biased to -300 V, acting simultaneously as a cold trap, reducing carbon deposition on the target surface, and electron suppressor.

The detector system consisted of a single, high efficiency (120% relative), high purity, coaxial germanium detector (HPGe) surrounded by a bismuth germanate (BGO) shield for active Compton background suppression. The detectors were mounted on a rail system at an angle of 45° relative to the beam, which allowed the detector to be easily moved to different distances from the target in order to make summing correction measurements during the calibration as well as increase the efficiency throughout the resonance scans. In the following, “close geometry” and “far geometry” refer to the distances between target and end cap of the HPGe detector of 1 and 20 cm, respectively.

The absolute efficiency of the detector was calibrated using ^{137}Cs and ^{152}Eu standard sources. To improve the efficiency calibration for high-energy γ -ray transitions, relative efficiencies for γ -ray transitions of an in-house produced ^{56}Co source as well as from the decay of the $E_r = 992$ keV resonance in the $^{27}\text{Al}(p, \gamma)^{28}\text{Si}$ reaction were scaled to the absolute efficiencies from the standard sources. Transition intensities were adopted from Antilla *et al.* [26] for the decay of the $E_r = 992$ keV resonance in the $^{27}\text{Al}(p, \gamma)^{28}\text{Si}$ reaction and from Bé *et al.* [27] for all other cases. The calculated efficiencies were fit with a double exponential function for

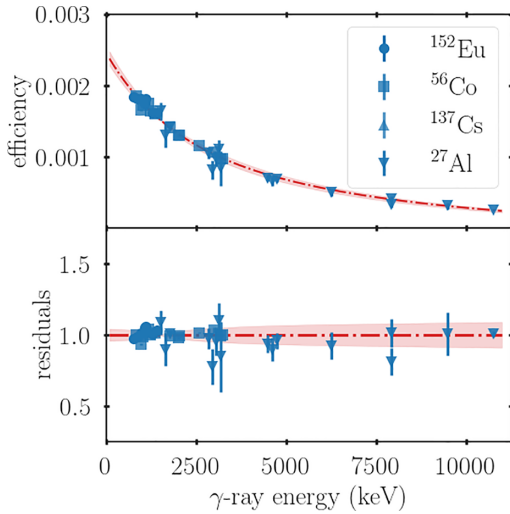


FIG. 3. The top panel shows the measured efficiencies of standard calibration sources ^{152}Eu and ^{137}Cs together with scaled relative efficiencies from an in-house produced ^{56}Co source and the decay transitions of the 992 keV resonance of the $^{27}\text{Al}(p, \gamma)^{28}\text{Si}$ reaction. The calculated efficiencies were fitted by a double exponential function, which was later used for interpolation. The bottom-panel shows the residuals of the measured values to the obtained fit function. The red bands indicate the 68% confidence limits of the fit.

interpolation purposes. The efficiency measurements, the fit function and its residuals are shown in Fig. 3. The energy calibration of the γ -ray spectra was performed using the same transitions, with an estimated uncertainty of 1 keV.

The first phase of the experiment started with a target scan of the $E_r = 828$ keV resonance for the aforementioned monitoring of the target stability (see Sec. III A) using the high yield $E_\gamma = 3.736$ MeV γ ray from the de-excitation of the second excited state to the ground state in ^{40}Ca . Following this, the thick-target yield plateaus of the $E_r = 1347$ and 1133 keV resonances were scanned in close geometry using the transitions to the ground state, to the state at $E_x = 3.736$ MeV,

its subsequent γ decay to the ground state, and the secondary decay of the state at $E_x = 3.906$ MeV to the ground state. This was followed by long measurements in far geometry to obtain the branching ratios in the γ cascade as well as the resonance strengths. The strengths of the two resonances, as well as that of the $E_r = 2043$ keV resonance, were measured absolutely by Cheng *et al.* [15]. Later measurements by Kikstra *et al.* [16] and Meißner [17] were obtained relative to the measurements of Cheng *et al.* [15]. In the following, long measurements were also carried out in far geometry for the resonances at $E_r = 783, 683, 667,$ and 622 keV. Note that the $E_r = 667$ keV resonance was observed for the first time by Meißner [17] and was easily distinguishable from the $E_r = 683$ keV resonance in the present work through the ground-state transition, utilizing the high-resolution of the HPGe detector. An example γ -ray spectra for a high statistics run on the $E_r = 1347$ keV resonance is shown in Fig. 4.

For the second phase of the experiment, thicker targets (about $500 \mu\text{g}/\text{cm}^2$) were used, which had a corresponding energy loss of about 150 keV (see Sec. III A) when mounted at 45° with respect to the beam direction. In this configuration, the excitation curve for the $E_\gamma = 3.736$ MeV γ ray was used as a signature for lower energy resonances as shown in Fig. 5. Subsequently, this region was also scanned with a thin target in small energy steps to map the yield curve for the transitions to ground state, as well as the secondary transitions at $E_\gamma = 3.736$ and 3.906 MeV in more detail as shown in Fig. 6. Based on this scan, a number of additional lower energy resonances in the region below $E_p = 600$ keV could be identified (see Fig. 7).

IV. ANALYSIS AND RESULTS

In the following sections we will discuss the analysis of the various observed resonances in terms of resonance energies and the resonance strengths to determine their respective contributions to the reaction rate as defined in Eq. (1). We will first present our results with respect to previously observed

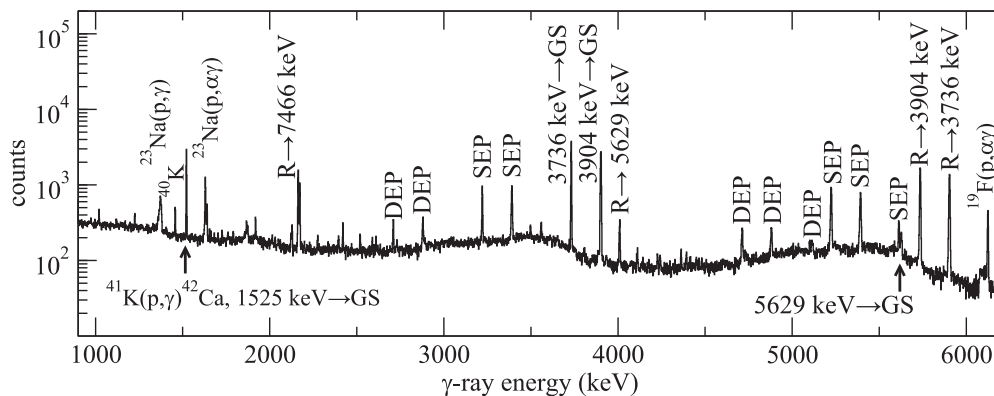


FIG. 4. Spectrum for the $E_r = 1347$ keV resonance in the $^{39}\text{K}(p, \gamma)^{40}\text{Ca}$ reaction using a thin target ($\Delta E \approx 25$ keV). The spectrum shown is for a measurement in the “close geometry” setup; for high statistics, branching ratios and strengths were calculated with “far geometry” measurements to avoid summing contributions. Background lines from proton induced reactions on Na and F contamination in the target material and backings are clearly visible. Many of the weak lines result from proton capture on ^{41}K (6.730%) that is present in the natural target material. Single escape (SEP) and double escape (DEP) peaks are also indicated.

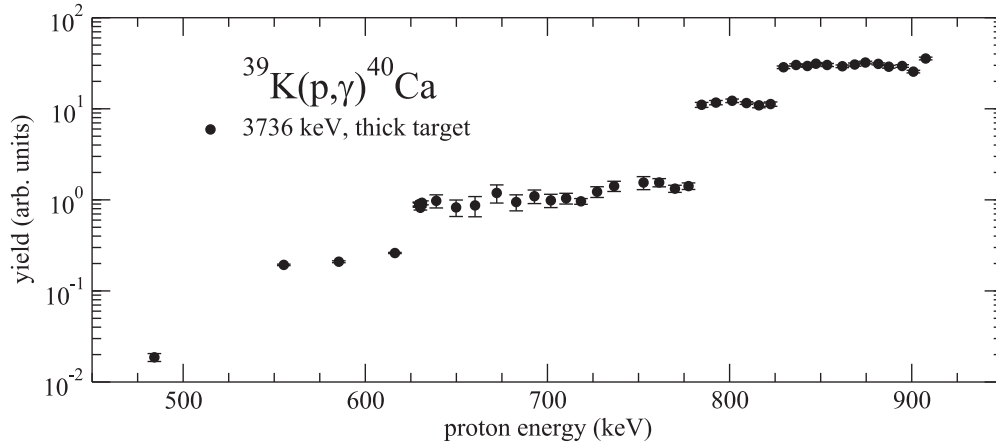


FIG. 5. Thick target yield for the second excited state to the ground state γ -ray line in ^{40}Ca at $E_\gamma = 3736$ keV. Steps in the yield curve as a function of increasing proton energy are indicative of new, strong, resonance contributions. The γ -ray spectra from three of the lowest energy measurements at $E_p = 484$, 555, and 616 keV are given in Fig. 7.

resonances followed by a discussion of the newly observed resonances of this work.

A. Resonances above $E_p = 600$ keV

The strengths of the observed resonances can be directly obtained from the on-resonance γ -ray yield measured on top of the resonance yield curve Y_{\max} . The resonance strength ($\omega\gamma$) results from the integration of the Breit-Wigner cross section over the target thickness or energy loss of the incident protons [25] and is expressed by

$$\omega\gamma = \frac{2Y_{\max}\epsilon_{\text{eff}}}{\lambda_r^2 b_\gamma \eta_\gamma}, \quad (2)$$

where ϵ_{eff} is the stopping power of the protons in the target material, λ_r the de Broglie wavelength of the proton at the resonance energy, b_γ the branching ratio of the γ -decay listed in Table I, and η_γ the efficiency of the HPGe detector at the corresponding γ -ray energy.

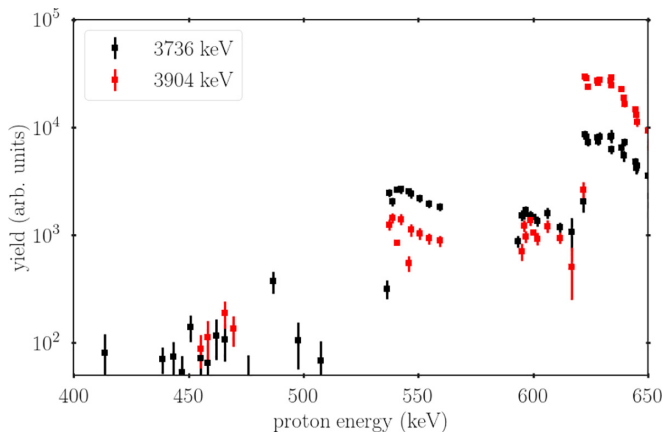


FIG. 6. Thin target energy scan in the region of the newly identified resonance candidates. Plateaus were clearly visible for the candidates at $E_r = 536$ and 596 keV. However, no plateaus were observed at lower energies.

The transitions used for the determination of the maximum yield are given in Table I. The effective stopping power (ϵ_{eff}) for protons in the target material was calculated with SRIM [28], but the direct comparison with previous data suggest that the stoichiometry of the target composition K_2WO_4 may have changed in the evaporation process. For this reason, the resonance strengths were calculated relative to those of the two resonances at $E_r = 1133$ and $E_r = 1347$ keV, measured absolutely by Cheng *et al.* [15] and already used for relative measurements by Kikstra *et al.* [16] and in the analysis by Longland *et al.* [22]. A scaling factor was determined for each of the two energies and then the weighted average was used for the normalization. The resulting resonance strengths for each of the directly observed resonances are listed in Table I.

B. Resonances below $E_p = 600$ keV

In the recent evaluation of the $^{39}\text{K}(p, \gamma)^{40}\text{Ca}$ reaction rate by Longland *et al.* [22], properties of several unobserved resonances are summarized. Given the estimated thickness of about 150 keV for the thick targets used in the second phase of the experiment, nine of those unobserved resonances were expected in the energy range between 330 and 600 keV. Four were observed.

Figure 7 shows the high-energy part of the spectra taken at the proton energies $E_p = 616$, 555, and 484 keV. Primary γ -ray transitions for four of the predicted resonances at $E_r = 596$, 536, 431 and 346 keV, as listed in Table III, are indicated, corresponding to γ energies of $E_\gamma = 5003$, 8858, 8755 and 8671 keV, respectively (see Table I). The two strong secondary γ -ray transitions from the 3736 and 3904 keV second and third final states to ground state, respectively, are always clearly visible. The secondary transition from the first excited state at 3353 keV to the ground state is forbidden as it is a $0^+ \rightarrow 0^+$ transition. The inset in Fig. 7(a) highlights the clearly visible $E_\gamma = 5003$ keV line from the $E_r = 596$ keV resonance, where no primary transition to the ground state was observed. Many weaker γ -ray lines are identified as beam induced background from the $^{41}\text{K}(p, \gamma)^{42}\text{Ca}$ reaction on the ^{41}K material in the natural abundance

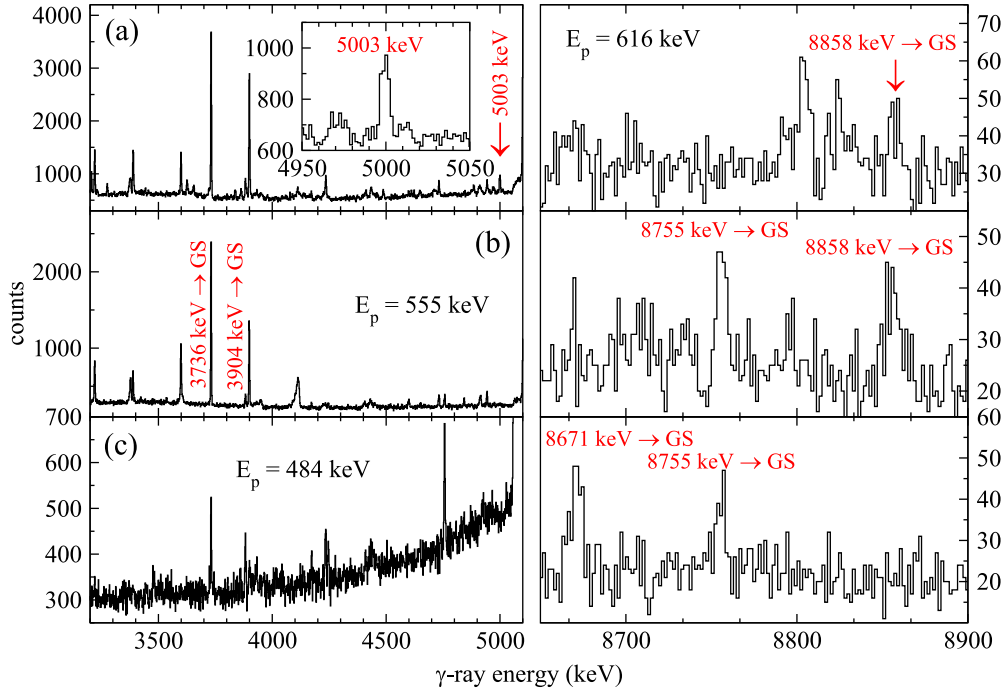


FIG. 7. Thick-target γ -ray spectra taken at three different proton beam energies: (a) 616, (b) 555, (c) 484 keV. Note the split in the spectra energy scales made to highlight the important low and high energy regions. Primary γ -ray transitions for four of the predicted resonances at $E_r = 596, 536, 431,$ and 346 keV are indicated, corresponding to characteristic γ -rays at $E_\gamma = 5003, 8858, 8755,$ and 8671 keV, respectively (see Table I). The two strong secondary γ -ray transitions from the 3736 and 3904 keV second and third final states to ground state, respectively, are always clearly visible. The secondary transition from the first excited state at 3353 keV to the ground state is forbidden as it is a $0^+ \rightarrow 0^+$ transition. The inset in (a) highlights the clearly visible $E_\gamma = 5003$ keV line from the $E_r = 596$ keV resonance, where no primary ground state transition was observed. Many weaker γ -ray lines are also present from reactions on $^{41}\text{K}(p, \gamma)^{42}\text{Ca}$ from the natural abundance potassium target material.

TABLE I. Resonance strengths between 330 and 1350 keV. Listed are the resonance energies E_r in the laboratory system and the excitation energies as derived from previous studies, the excitation energy of the final state E_f , the γ -ray energy of the corresponding γ -ray transition E_γ , as well as relative resonance strengths. γ -ray energies have been corrected for Doppler and recoil shifts.

E_r (keV)	E_x (keV)	E_f (keV)	E_γ (keV)	b_γ	$\omega\gamma_{\text{rel}}$ (meV)
1346.58(13) ^a	9640.89(7)	3736.69(5)	5917(2)	0.390(05) ^a	474(36)
1132.8(4) ^a	9432.46(18)	0.0	9430(2)	0.910(30) ^b	203(19)
828.27(11) ^a	9135.66(5)	3736.69(5)	5396(2)	0.587(09) ^a	34(3)
783.23(11) ^a	9091.70(6)	3736.69(5)	5352(2)	0.581(10) ^a	17(3)
683.45(15) ^a	8994.5(11)	0.0	8995(2)	0.746(16) ^a	12(2)
667(6) ^c	8978(6)	0.0	8981(2)	1.000 ^d	6.1(6)
622.23(12) ^a	8935.8(9)	0.0	8934(2)	0.290(20) ^a	8.5(11)
595.5(9) ^c	8909.0(9)	3904.38(3)	5003(2)	0.50(10) ^e	0.04(1)
535.6(9) ^c	8850.6(9)	0.0	8858(2)	0.042(10) ^e	0.139(20)
535.6(9) ^c	8850.6(9)	3904.38(3)	3904(2) ^f	0.352(20) ^e	0.138(14)
535.6(9) ^c	8850.6(9)	3736.69(5)	3736(2) ^f	0.352(20) ^e	0.141(14)
430.54(9) ^c	8748.22(9)	0.0	8755(2)	1.000 ^e	0.004(1)
345.5(8) ^c	8665.3(8)	0.0	8671(2)	1.000 ^e	0.004(1)

^aFrom Kikstra *et al.* [16].

^bFrom Cheng *et al.* [15].

^cFrom Longland *et al.* [22].

^dFrom Meißner [17].

^eThe branchings for the resonances below $E_p = 600$ keV are taken from the present analysis as described in the text.

^fFor the resonance at $E_r = 536$ keV only the secondary transitions at 3909 and 3734 keV could be analyzed.

potassium target. This reduces the number of significant resonance contributions in this excitation range considerably compared to those predicted from the statistical analysis of Longland *et al.* [22].

The lower energy range of the spectra shows large beam induced background radiation from the ^{12}C and ^{19}F contamination of the target material, leading to strong γ -ray emission from the $^{12}\text{C}(p, \gamma)^{13}\text{N}$ and $^{19}\text{F}(p, \alpha\gamma)^{16}\text{O}$ reactions over the γ -ray energy range between 2 and 3 MeV as well as between 5.5 and 7.5 MeV. This background handicaps the analysis of the lowest energy resonance spectra. The resonance decay is characterized by direct and cascade decay of the populated compound states to the 3.904 MeV 2^+ third excited state, and to the 3.736 MeV 3^- second excited state as well as by the direct decay to the 0^+ ground state in ^{40}K . The strong background also prevents a reliable analysis of weaker transitions to higher excited states in the 5 to 6 MeV excitation range of ^{40}Ca . The determination of the resonance strengths therefore relies on the analysis of the direct ground state transition and the secondary γ transitions of the 3.906 and 3.743 MeV states to the ground state, which reflect the strengths of the γ -ray cascades.

A thick-target yield curve for the secondary transition of the second excited state $J^\pi = 3^-$ at 3736 keV in ^{40}Ca is shown in Fig. 5. The observed energy range is between 480 and 910 keV. The steps clearly indicate the strength of the contributions of a number of the resonances in that energy range. In addition to the previously observed higher energy resonances at $E_r = 828, 783,$ and 622 keV, the thick target yield of the two lower energy resonances at $E_r = 536$ and 431 keV can be identified. These resonances are also confirmed in an energy scan using a thin target, as shown in Fig. 6, for the ground state transition of the second excited state at 3736 keV and the third excited state at 3904 keV. This scan also confirms the observation of a weak resonance at $E_r = 596$ keV in both transitions.

The resonances identified here correspond well to some of the ^{40}Ca unbound states that have been observed previously in $^{39}\text{K}(^3\text{He}, d)^{40}\text{Ca}$ single-particle transfer reactions at 16 MeV by Meißner [17]. The spectral resolution of these studies was about 16 keV, considerably poorer than the resolution of HPGe detectors but still sufficient to distinguish the difference between the low energy states in question. These results have been taken into account in the spin considerations for the observed states and the resonance strengths tabulated in Table I.

For the decay of the resonance at $E_r = 596$ keV ($E_x = 8.909$ MeV), a γ transition to the third excited state at 3.904 MeV (2^+), with a weaker branch to the 3.736 MeV (3^-) state, is observed as shown in Fig. 6. This is in agreement with the $J = 0$ assignment for the level suggested by Longland *et al.* [22].

For the resonance at $E_r = 536$ keV ($E_x = 8.851$ MeV), the ground state transition could be clearly identified. This questions the high spin values of $J^\pi = 6^-, 7^-,$ or 8^- suggested by Longland *et al.* [22]. This assignment is based on angular distribution analysis of inelastic proton scattering data on ^{40}Ca , measured at bombarding energies between 24 and 40 MeV [29]. However, as their Fig. 4 indicates, this level corresponds to a very weak peak within a multiplicity of highly

excited states in the inelastic proton scattering spectrum. The angular distribution data may well be influenced by the tails of neighboring states. Despite a decomposition effort in the spectral analysis, it is possible that the spin assignment of this state could have been compromised by the impact of a neighboring higher spin state at $E_x = 8.978$ MeV, which has not been observed as a resonance in the present radiative capture study. Unpublished angular distribution data of the $^{39}\text{K}(^3\text{He}, d)^{40}\text{Ca}$ proton transfer reaction [17] does indeed match a lower spin assignment. This is also supported by thin target measurements reported here, which show transitions to the 3.736 (3^-) and the 3.904 MeV (2^+) lower excited states. The observed γ -transition suggests a 35% branching to the 2^+ state at 3904 keV with the subsequent ground state transition and a 61% feeding of the 3^- state at 3736 keV with the subsequent ground state transition. This suggests a spin-parity range between 1^- and 3^- for this level.

The ground state transition for the resonance at $E_r = 431$ keV ($E_x = 8.748$ MeV) was observed, which supports the 2^+ assignment given in the literature [22,23]. No other transitions to excited states in ^{40}Ca could be identified. This was also confirmed in a recent nuclear fluorescence experiment at the HI γ S facility at TUNL [30]. We therefore adopt a 100% $E2$ ground state transition for the decay.

For the resonance at $E_r = 346$ keV ($E_x = 8.665$ MeV) the transition to the ground state was observed, which indicates that this resonance corresponds to the 1^- state tabulated with $E_x = 8.6653(8)$ MeV by Chen [23]. This state does not decay via the levels at 3.736 (3^-) and 3.904 MeV (2^+) as shown in Fig. 6, which is consistent with the given spin-parity assignment and the assumption of a 100% $E1$ ground state transition.

The resonance strengths for these low energy resonances listed in Tables I and II are calculated on the basis of a 100% branching to the final state identified in Table I. Additional transitions will enhance the given values when a more complete γ -decay pattern can be measured.

V. REACTION RATE ANALYSIS

The reaction rate for the $^{39}\text{K}(p, \gamma)^{40}\text{Ca}$ reaction was derived using the narrow resonance approximation given by Eq. (1). The resonance strengths for the states observed here between $E_p = 1400$ and 600 keV were taken from Table II. For the resonances below $E_p = 600$ keV proton energy, the resonance strengths were derived from the strength of the ground state transitions and the secondary transitions from the 3.904 and the 3.736 MeV states to the ground state. These branchings carry the bulk of the decay strength. A more complex branching scheme might increase the resonance strength by up to 15%, which is within the range of uncertainty. The reaction rate derived from the strengths of the present work is presented in the Supplemental Material [31].

Figure 8 shows the reaction rate contributions of the resonance states discussed here as a function of temperature, while Fig. 9 shows the reaction rate and its strongest resonance components relative to that of Longland *et al.* [22]. The rate of Longland *et al.* [22] is consistently higher than the total

TABLE II. Comparison of resonance strengths obtained from this work to values from previous measurements by Cheng *et al.* [15], Leenhouts [14], Kikstra *et al.* [16], and the unpublished results by Meißner [17].

E_r (keV)	J^π [16,17,23]	$\omega\gamma$ (meV) Cheng <i>et al.</i> [15]	$\omega\gamma$ (meV) Kikstra <i>et al.</i> [16]	$\omega\gamma$ (meV) Leenhouts [14]	$\omega\gamma$ (meV) Meißner [17]	$\omega\gamma$ (meV) this work
1346.58(13) ^a	3 ⁻	513(63)	625(250)	637(26)		474(36)
1132.8(4) ^a	2 ⁺	200(25)	325(138)	250(100)		203(19)
828.27(11) ^a	(2, 3) ⁻	40(12)	75(25)	25(10)		34(3)
783.23(11) ^a	3 ⁻	14(4)	35(14)	13(5)		17(3)
683.45(15) ^a	2 ⁺		19(8)		19(3)	12(2)
667(6) ^b	2 ⁺				10(1)	6.1(6)
622.23(12) ^a	2 ⁺		11(5)		13(2)	8.4(12)
595.5(9) ^b	0 ⁺				<0.390	0.04(1)
535.6(9) ^b	(1 ⁻ , 3 ⁻)				<0.220	0.140(14)
430.54(9) ^b	2 ⁺				<0.071	0.004(1)
345.5(8) ^b	(1 ⁻)				<0.035	0.004(1)

^aFrom Kikstra *et al.* [16].

^bFrom Longland *et al.* [22] and references therein.

rate obtained here. For the low and high temperature extremes, the difference might be explained by the neglect of very low and high energy resonances not observed in this study. In the medium temperature range of nova burning considered here, the difference is more likely due to the assumption of too high of a resonance density. The results of Longland *et al.* [22] were based on the observed density of unbound states in ⁴⁰Ca and the assumption of singleparticle strengths for all possible contributing states in the double closed shell nucleus ⁴⁰Ca. Figure 9 shows that the reaction rate in the temperature

range of novae is dominated by the $E_r = 346$ and 536 keV resonances.

Possible direct capture contributions were calculated in the framework of a potential model using the code JEZEBEL [32]. The total cross section for this transition depends on the single-particle strengths of the final states, which were taken from the literature [17,23]. For the potential model, an adaptive Wood-Saxon potential was used with a radius $r = r_0 A^{1/3}$, $A = 39$, $r_0 = 1.26$ fm, and a diffuseness of $a = 0.65$ fm. The results provide a cross section and reaction rate

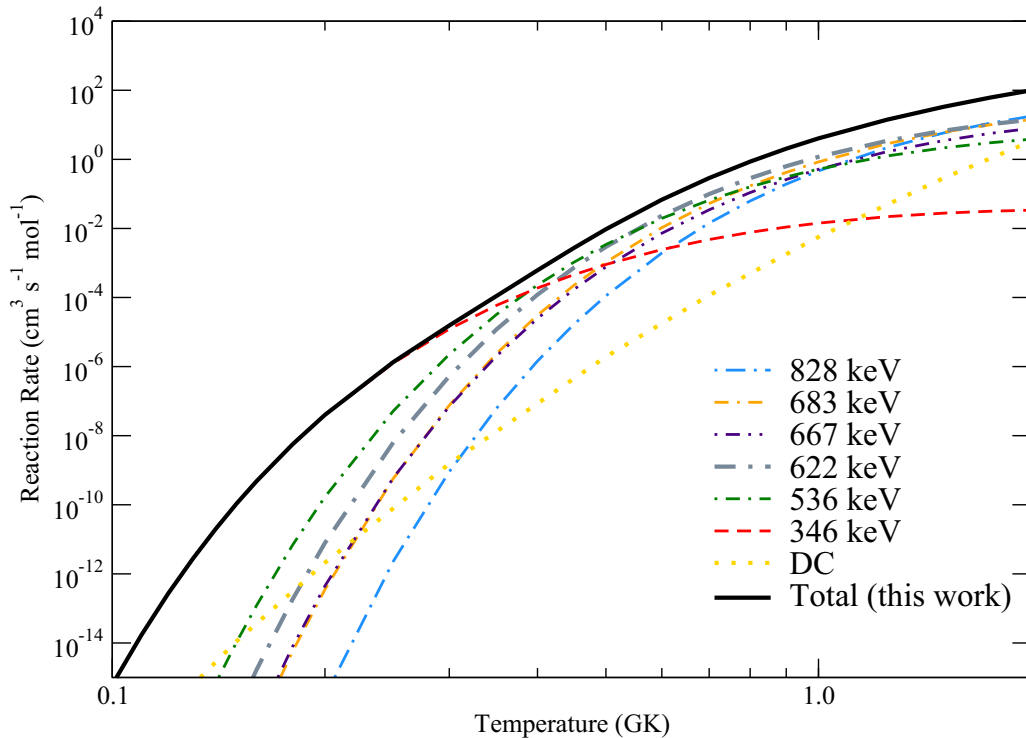


FIG. 8. Reaction rate components for the $^{39}\text{K}(p, \gamma)^{40}\text{Ca}$ reaction over the temperature range applicable for a novae environment. An estimate of the direct capture (DC) contribution is also shown for comparison. The model parameters are given in the text.

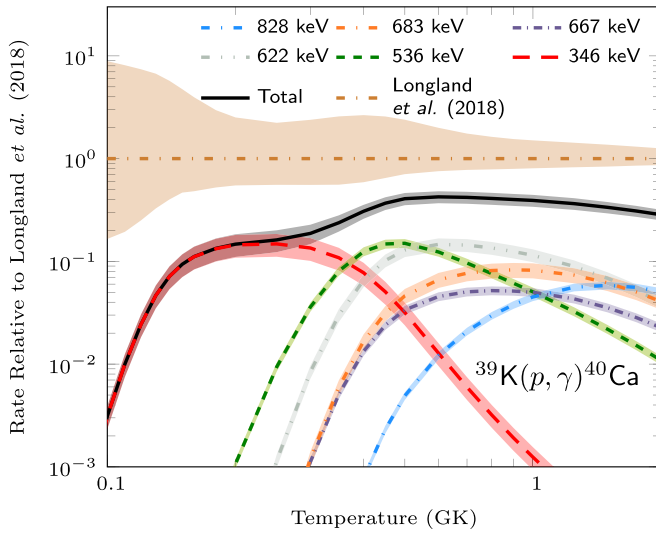


FIG. 9. Fractional contribution of the strongest narrow resonances that dominate the $^{39}\text{K}(p, \gamma)^{40}\text{Ca}$ reaction rate. The total rate and the individual resonance contributions are taken relative to the total rate of Longland *et al.* [22]. The uncertainty of Longland *et al.* [22] is also indicated for comparison.

component that is negligible compared to the resonant contributions shown in Fig. 8 over the entire temperature range.

Finally, to illustrate the level of precision of the Hauser-Feshbach (HF) model in estimating the reaction rate for the $^{39}\text{K}(p, \gamma)^{40}\text{Ca}$ reaction, the HF reaction rate was calculated using the codes SAPHIRE [33] and taken from the NON-SMOKER HF library of Rauscher and Thielemann [34,35]. The HF reaction rates are shown relative to that of Longland *et al.* [22] in Fig. 10. Both HF rates significantly overestimate the reaction rate compared to that of this work over the entire temperature range of interest, with that of Rauscher and Thielemann [34,35] coming closest to the present rate

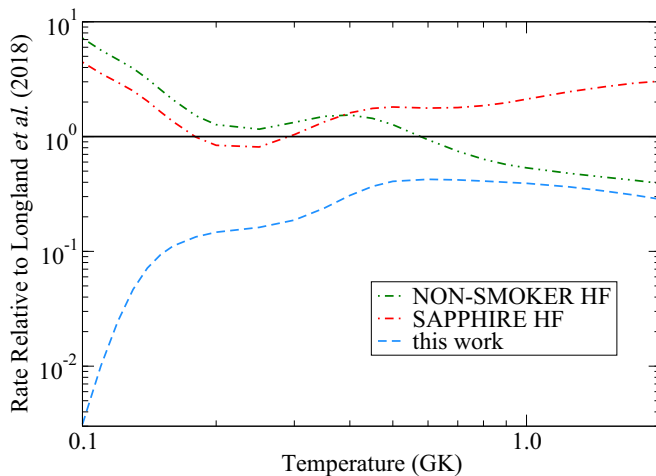


FIG. 10. Ratio the $^{39}\text{K}(p, \gamma)^{40}\text{Ca}$ reaction rate of the present work (blue dashed line) as well as from statistical model predictions using SAPHIRE [33] (red dashed line) and NON-SMOKER [34,35] relative to the rate of Longland *et al.* [22].

TABLE III. Resonance energies (in the laboratory frame of reference) and γ transitions to the ^{40}Ca ground state, observed in the spectra of the thick target runs at lower energies. These transitions provide information about the energies of resonances below $E_p = 600$ keV that contribute to the $^{39}\text{K}(p, \gamma)^{40}\text{Ca}$ reaction. For comparison, corresponding levels reported in the compilation [23] and resonance energies (in the center-of-mass frame) of previously predicted candidate resonances from Longland *et al.* [22] are also given.

E_p (keV)	E_γ (keV)	E_x (keV) [23]	E_r (keV) [22]
595.5(9)	8915(2)	8909.0(9)	580.6(9)
535.6(9)	8858(2)	8850.6(9)	522.2(9)
446.9(6)		8764.18(6)	435.7(6)
430.54(9)	8755(2)	8748.22(9)	419.8(9)
399(8)		8717(8)	389(8)
382.2(10)		8701(1)	372.6(10)
358.82(10)		8678.29(10)	349.85(10)
345.5(8)	8671(2)	8665.3(8)	336.9(8)

above 1 GK, where it only overestimates by $\approx 30\%$. The overestimation likely signals that the level density in the HF calculations is overestimated. It should be noted that Rauscher and Thielemann [34,35] indicate that their HF model should not be used below 0.18 GK, which is where the largest discrepancies occur.

VI. CONCLUSION

This paper investigates the contributions and strength of the $^{39}\text{K}(p, \gamma)^{40}\text{Ca}$ reaction rate near the closure of the sd shell, which has been considered a likely endpoint of nova nucleosynthesis [1]. This reaction may play a role in high temperature nova environments of $0.2 \lesssim T \lesssim 0.3$ GK for exploring the possibility of an extended hydrogen burning pattern ranging beyond the sd shell and the double-closed-shell nucleus ^{40}Ca [10]. The experimental results (see Table III and Fig. 8) demonstrate that the single-particle strength distribution in the unbound excitation range of the ^{40}Ca compound nucleus is up to an order of magnitude smaller than previously assumed by Longland *et al.* [22] on the basis of statistical considerations. It is also smaller than predictions in the framework of the HF model based on a smooth level density function calculated with the back-shifted Fermi-gas model [33], which overestimates the level density.

The results presented here indicate that the reaction rate for the $^{39}\text{K}(p, \gamma)^{40}\text{Ca}$ reaction over the range $0.1 \lesssim T \lesssim 0.5$ GK—the typical range for peak temperature conditions in novae—is dominated by the contributions of the two resonances at $E_r = 346$ and $E_r = 536$ keV. Other resonances in that energy range below 600 keV, such as the $E_r = 431$ and 596 keV resonances, are considerably weaker. Longland *et al.* [22] suggests strong contributions from lower energy resonances, but only upper limits were given for the proton widths based on rather large single particle structure assumptions. The proton transfer studies by Meißner [17] suggested that states at $E_x = 8665$ and 8551 keV as well as a state

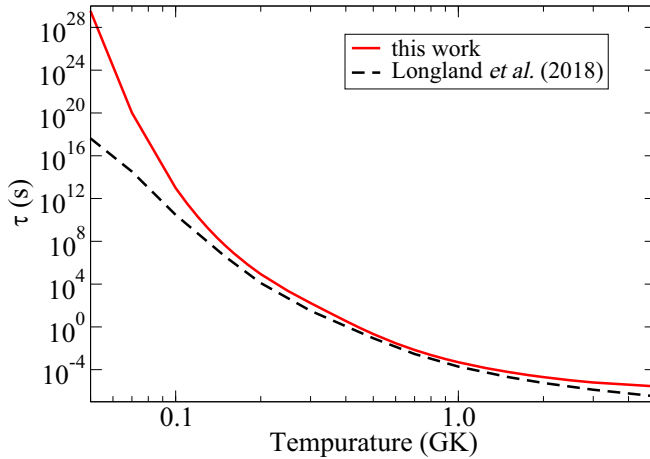


FIG. 11. Comparison of the lifetime of ^{39}K under novae conditions as a function of temperature using either the present rate (red solid line) or that of Longland *et al.* [22] (black dashed line).

at $E_x = 8425$ keV are being populated. These would correspond to the resonance observed here at $E_p = 346$ keV and two lower resonances at $E_p = 220 \pm 16$ and 100 ± 10 keV, respectively, which have not yet been observed in radiative capture studies. These resonances are expected to dominate the temperature range $T \leq 0.1$ GK, as suggested by Longland

et al. [22], and need to be studied in more detail in future low energy accelerator experiments. In the peak temperature range of novae discussed here, $T \geq 0.1$ GK, their contribution is negligible since the lifetime of ^{39}K at such temperatures is in the range of several hundred years, too long for the lifetime of a nova event. Figure 11 shows the lifetime (τ) of ^{39}K versus proton capture,

$$\tau(^{39}\text{K}) = \frac{1}{X_{\text{H}} \rho N_A \langle \sigma v \rangle}, \quad (3)$$

with $X_{\text{H}} \approx 0.5$ as the mass fraction of hydrogen and $\rho \approx 10^3$ g/cm 3 being the density. This figure demonstrates that, in the temperature range $0.2 \lesssim T \lesssim 0.3$ GK, the lifetime decreases from 1 h to 2 s, which makes the production of ^{40}Ca at nova peak temperatures feasible. For longer lived hydrogen-rich burning environments, the contribution of the lower energy resonances needs to be investigated.

ACKNOWLEDGMENTS

This research utilized resources from the Notre Dame Center for Research Computing and was funded by the National Science Foundation through Grant No. PHY-2011890 (University of Notre Dame Nuclear Science Laboratory) and Grant No. PHY-1430152 (the Joint Institute for Nuclear Astrophysics - Center for the Evolution of the Elements).

- [1] J. José and M. Hernanz, Nucleosynthesis in classical novae: CO versus ONe white dwarfs, *Astrophys. J.* **494**, 680 (1998).
- [2] M. Wiescher, J. Görres, E. Uberseder, G. Imbriani, and M. Pignatari, The cold and hot CNO cycles, *Annu. Rev. Nucl. Part. Sci.* **60**, 381 (2010).
- [3] L. Zhang, J. He, R. J. deBoer, M. Wiescher, A. Heger, D. Kahl, J. Su, D. Odell, Y. Chen, X. Li, J. Wang, L. Zhang, F. Cao, H. Zhang, Z. Zhang, X. Jiang, L. Wang, Z. Li, L. Song, H. Zhao *et al.*, Measurement of $^{19}\text{F}(p, \gamma)^{20}\text{Ne}$ reaction suggests CNO breakout in first stars, *Nature (London)* **610**, 656 (2022).
- [4] A. Boeltzig, R. J. deBoer, Y. Chen, A. Best, M. Couder, A. Di Leva, B. Frenzt, J. Görres, G. Gyürky, G. Imbriani, M. Junker, Q. Liu, S. Lyons, K. Manukyan, K. T. Macon, L. Morales, M. T. Moran, D. Odell, C. Seymour, G. Seymour *et al.*, Investigation of direct capture in the $^{23}\text{Na}(p, \gamma)^{24}\text{Mg}$ reaction, *Phys. Rev. C* **106**, 045801 (2022).
- [5] J. G. Ross, J. Görres, C. Iliadis, S. Vouzoukas, M. Wiescher, R. B. Vogelaar, S. Utku, N. P. T. Bateman, and P. D. Parker, Indirect study of low-energy resonances in $^{31}\text{P}(p, \alpha)^{28}\text{Si}$ and $^{35}\text{Cl}(p, \alpha)^{32}\text{S}$, *Phys. Rev. C* **52**, 1681 (1995).
- [6] C. Iliadis, J. Görres, J. Ross, K. Scheller, M. Wiescher, C. Grama, T. Schange, H. Trautvetter, and H. Evans, Explosive hydrogen burning of ^{31}P , *Nucl. Phys. A* **559**, 83 (1993).
- [7] C. Iliadis, U. Giesen, J. Görres, M. Wiescher, S. Graff, R. Azuma, and C. Barnes, Direct proton capture on ^{32}S , *Nucl. Phys. A* **539**, 97 (1992).
- [8] C. Iliadis, J. Görres, J. Ross, K. Scheller, M. Wiescher, R. Azuma, G. Roters, H. Trautvetter, and H. Evans, Explosive hydrogen burning of ^{35}Cl , *Nucl. Phys. A* **571**, 132 (1994).
- [9] C. Iliadis, J. G. Ross, J. Görres, M. Wiescher, S. M. Graff, and R. E. Azuma, Reaction $^{36}\text{Ar}(p, \gamma)^{37}\text{K}$ in explosive hydrogen burning, *Phys. Rev. C* **45**, 2989 (1992).
- [10] J. José and M. Hernanz, Nucleosynthesis in classical nova explosions, *J. Phys. G: Nucl. Part. Phys.* **34**, R431 (2007).
- [11] R. Das, Elemental abundances in novae, *J. Astrophys. Astron.* **42**, 13 (2021).
- [12] R. D. Gehrz, J. W. Truran, R. E. Williams, and S. Starrfield, Nucleosynthesis in classical novae and its contribution to the interstellar medium, *Publ. Astron. Soc. Pac.* **110**, 3 (1998).
- [13] H. Leenhouts and P. Endt, Gamma decay of levels in ^{40}Ca measured with the $^{39}\text{K}(p, \gamma)^{40}\text{Ca}$ reaction, *Physica* **32**, 322 (1966).
- [14] H. Leenhouts, Spins and parities of levels in ^{40}Ca measured with the $^{39}\text{K}(p, \gamma)^{40}\text{Ca}$ reaction, *Physica* **35**, 290 (1967).
- [15] C. W. Cheng, S. K. Saha, J. Keinonen, H. B. Mak, and W. McLatchie, Hydrogen burning of ^{39}K in explosive oxygen burning, *Can. J. Phys.* **59**, 238 (1981).
- [16] S. Kikstra, C. Van Der Leun, P. Endt, J. Booten, A. van Hees, and A. Wolters, The ^{40}Ca level scheme investigated with the $^{39}\text{K}(p, \gamma)^{40}\text{Ca}$ reaction, *Nucl. Phys. A* **512**, 425 (1990).
- [17] J. Meißner, Untersuchung von Zuständen in Ca-40 nahe der Protonenschwelle und deren Einfluß auf den Reaktionsfluß im explosiven Wasserstoffbrennen, Diplomarbeit, Technische Universität München, 1993 (unpublished).
- [18] H. Fuchs, K. Grabisch, and G. Röscher, Investigation of states in ^{40}Ca by the $^{39}\text{K}(d, n)$ reaction, *Nucl. Phys. A* **129**, 545 (1969).
- [19] J. R. Erskine, Energy-level structure of Ca^{40} as observed with the $\text{K}^{39}(\text{He}^3, d)\text{Ca}^{40}$ reaction, *Phys. Rev.* **149**, 854 (1966).

- [20] K. K. Seth, J. A. Biggerstaff, P. D. Miller, and G. R. Satchler, Study of proton particle-hole states in ^{40}Ca by the $^{39}\text{K}(^3\text{He}, d)^{40}\text{Ca}$ reaction, *Phys. Rev.* **164**, 1450 (1967).
- [21] M. E. Cage, R. R. Johnson, P. D. Kunz, and D. A. Lind, The $^{39}\text{K}(^3\text{He}, ^3\text{He})^{39}\text{K}$ and $^{39}\text{K}(^3\text{He}, d)^{40}\text{Ca}$ reactions at 29.3 MeV, *Nucl. Phys. A* **162**, 657 (1971).
- [22] R. Longland, J. Dermigny, and C. Marshall, Reaction rates for the $^{39}\text{K}(p, \gamma)^{40}\text{Ca}$ reaction, *Phys. Rev. C* **98**, 025802 (2018).
- [23] J. Chen, Nuclear data sheets for $A = 40$, *Nucl. Data Sheets* **140**, 1 (2017).
- [24] W. A. Fowler, G. R. Caughlan, and B. A. Zimmerman, Thermonuclear reaction rates, II, *Annu. Rev. Astron. Astrophys.* **13**, 69 (1975).
- [25] W. A. Fowler, C. C. Lauritsen, and T. Lauritsen, Gamma-radiation from excited states of light nuclei, *Rev. Mod. Phys.* **20**, 236 (1948).
- [26] A. Antilla, J. Keinonen, M. Hautala, and I. Forsblom, Use of the $^{27}\text{Al}(p, \gamma)^{28}\text{Si}$, $E_p = 992$ keV resonance as a gamma-ray intensity standard, *Nucl. Instrum. Methods* **147**, 501 (1977).
- [27] M.-M. Bé, V. Chechev, R. Dersch, O. A. M. Helene, R. G. Helmer, M. Herman, S. Hlaváč, A. Marcinkowski, G. Molnár, A. Nichols, E. Schönfeld, V. R. Vanin, and M. J. Woods, Recommended decay data, high energy gamma ray standards and angular correlation coefficients, in *Update of X Ray and Gamma Ray Decay Data Standards for Detector Calibration and Other Applications*, Vol. 1 (IAEA, Vienna, 2007).
- [28] J. F. Ziegler, M. D. Ziegler, and J. P. Biersack, SRIM - The stopping and range of ions in matter (2010), *Nucl. Instrum. Methods Phys. Res., Sect. B* **268**, 1818 (2010).
- [29] C. R. Gruhn, T. Y. T. Kuo, C. J. Maggiore, H. McManus, F. Petrovich, and B. M. Preedom, Energy dependence of proton inelastic scattering from ^{40}Ca , *Phys. Rev. C* **6**, 915 (1972).
- [30] D. Gribble, C. Iliadis, R. V. F. Janssens, U. Friman-Gayer, Krishichayan, and S. Finch, Investigation of ^{11}B and ^{40}Ca levels at 8–9 MeV by nuclear resonance fluorescence, *Phys. Rev. C* **106**, 014308 (2022).
- [31] See Supplemental Material at <http://link.aps.org/supplemental/10.1103/PhysRevC.107.065806> for the tabulated reaction rate.
- [32] M. Wiescher, H. Becker, J. Görres, K.-U. Kettner, H. Trautvetter, W. Kieser, C. Rolfs, R. Azuma, K. Jackson, and J. Hammer, Nuclear and astrophysical aspects of $^{18}\text{O}(p, \gamma)^{19}\text{F}$, *Nucl. Phys. A* **349**, 165 (1980).
- [33] M. Beard, E. Uberseder, R. Crowter, and M. Wiescher, Comparison of statistical model calculations for stable isotope neutron capture, *Phys. Rev. C* **90**, 034619 (2014).
- [34] T. Rauscher and F.-K. Thielemann, Astrophysical reaction rates from statistical model calculations, *At. Data Nucl. Data Tables* **75**, 1 (2000).
- [35] T. Rauscher and F.-K. Thielemann, Tables of nuclear cross sections and reaction rates: An addendum to the paper “Astrophysical reaction rates from statistical model calculations”, *At. Data Nucl. Data Tables* **79**, 47 (2001).